Astron. Astrophys. 342, 389–394 (1999)

ASTRONOMY AND ASTROPHYSICS

Research Note

Motion in a potential creating a weak bar structure

N.D. Caranicolas and G.I. Karanis

Section of Astrophysics, Astronomy and Mechanics Department of Physics, University of Thessaloniki, GR-54006 Thessaloniki, Greece

Received 13 March 1998 / Accepted 15 September 1998

Abstract. We investigate the properties of motion in a general galactic potential, found using a monoparametric family of ellipses and the Inverse Problem Theory. It is found, that an interesting case of the potential is that of two coupled perturbed elliptic oscillators. This potential represents a weak bar and it can describe the motion in the central parts of a barred galaxy. In the above potential we find the main families of orbits using a map in the non-rotating as well as in the rotating case. Comparing the results of the map, with those found by numerical integration, we find that the map describes very well the characteristic of motion in the non rotating case. Satisfactory results are also obtained when the galaxy rotates. Finally the onset of chaotic motion is studied and a comparison of the weak bars to strongly non axially symmetric bars is made.

Key words: galaxies: kinematics and dynamics

1. Introduction

Observations have shown that about 2/3 of disc galaxies are barred. Unfortunately one cannot observe the shape of orbits of stars inside a bar. Nevertheless N-body simulations have shown that orbits in bars may have different shapes (see Miller and Smith 1978). Based on a set of figure-eight orbits Caranicolas (1998) found, using the Inverse Problem techniques, a general potential which, among others, creates the above family of orbits. A special case of this potential is a two dimensional perturbed harmonic oscillator with ratio of unperturbed frequencies 1:2. This means that the unperturbed part of the potential was strongly non axially symmetric. In the following we shall use the term 'strong bar' for this potential. The above potential reproduced very well the figure-eight orbits. On the other hand, numerical calculations have shown (Caranicolas and Karanis 1998) that the potential produces also some other families of orbits in both non rotating and rotating cases. It was also found that chaos occurred when the perturbation was strong.

In this article we shall try to find the properties of motion in a potential based in a monoparametric family of ellipses. Our work has a compound character and it is organized as follows: In Sect. 2 we define the family of orbits and build up the potential by means of the Inverse Problem Theory. In Sect. 3 we construct a map, based on the averaged Hamiltonian, in both non rotating and rotating cases. With the aid of the map we study the properties of all orbits in the $x - p_x$ Poincare surface of section. We also compare the surface of section generated by the map to that found by numerical integration. In Sect. 4 we look for the onset of chaotic motion and compare the results to those found in Caranicolas and Karanis (1998). Finally, in Sect. 5, we present a discussion and the conclusion of this research.

Send offprint requests to: N.D.Caranicolas

2. The galactic potential

The method and the steps that we take to build up a potential, creating a monoparametric family of orbits, are given in detail in Caranicolas (1998) (see also Bozis and Borghero 1997). We present here only the results that are necessary. Here the family of orbits are ellipses given in parametric form by the Eqs.

$$x = 5b\cos\lambda \ , \ y = \sin\lambda/5 \tag{1}$$

where b is a small parameter $b \leq 0.2$. It is evident that ellipses of family (1) can form a bar structure. On the other hand it is widely known that one can find elliptical orbits in a self consistent barred potential. Such self consistent barred models are plenty in the literature (see for instance Combes et al. 1990, Miwa and Noguchi 1998).

The first three terms of the general potential, associated with the family (1) are

$$V(\lambda,b) = V_0(\lambda,b) + bV_{10}\cos^2\lambda + b^2[V_{20} - \frac{625}{4}(4V_0 + V_{0\lambda}\sin 2\lambda)]\sec^2\lambda \ , \tag{2}$$

where V_{10}, V_{20} are constants while $V_0, V_{0\lambda}$ are an arbitrary function and its first derivative with respect to λ. Taking $V_{10} = V_{20} = 0$ and

$$V_0 = V_{00}\cos^2\lambda - \epsilon\cos^4\lambda \ , \tag{3}$$

where V_{00} is a constant and $\epsilon > 0$ is a small parameter, we obtain

$$V = \frac{1}{2}\cos^2\lambda[-\epsilon + 2V_{00} - 1250b^2V_{00} + \epsilon(-1 + 1250b^2)\cos 2\lambda] \ , \tag{4}$$

which translated to x, y variables, for $V_{00} = -1/50$ reads

$$V = \frac{1}{2}(x^2+y^2) + \epsilon[25x^2 + 50y^2 - 1250x^2y^2 - 625y^4 - 1] - \frac{1}{50} \quad . \tag{5}$$

This potential is known as the perturbed elliptic oscillators (see Deprit 1990, Caranicolas and Innanen 1992). Furthermore, this potential describes the motion in the central parts of a non rotating barred galaxy because it is based in orbits creating a bar-like structure. It is evident that the bar is weak (see Binney and Tremaine 1987 p.146). In order to check whether potential (5) produces the ellipses (1) we work as follows: We choose $\lambda = 0$ and the orbit starts at $x_0 = 5b, y_0 = 0$, with $v_x = 0$ while v_y is found from the energy integral. For the above initial conditions the energy of the elliptic orbits is

$$E = \frac{25}{2}(1+50\epsilon)b^2 \tag{6}$$

The region on the $\lambda - b$ plane where the family of ellipses (1) exists is given by the inequality

$$1 + 50\epsilon\cos^2\lambda \geq 15625\epsilon b^2 \sin^2 2\lambda \quad , \tag{7}$$

which is always true for small values of ϵ and $b \leq 0.2$. Numerical experiments show that potential (5) produces very well the elliptic orbits when $b \leq 0.2$ and ϵ is of the order of 10^{-5}.

3. Orbits in a weak bar model

In addition to the elliptic orbits, potential (5) produces other families of orbits as well. In what follows we shall study the properties of orbits when the bar is non rotating and in the case where the bar rotates.

a) Non rotating case

The Hamiltonian to the potential (5) is

$$H = \frac{1}{2}(p_x^2 + p_y^2 + x^2 + y^2) + \epsilon[25x^2 + 50y^2 - 1250x^2y^2 - 625y^4 - 1] - \frac{1}{50} = h \quad , \tag{8}$$

where p_x, p_y are the momenta per unit mass conjugate to x,y and h is the numerical value of H.

In order to study the properties of orbits we shall use a map derived from the averaged Hamiltonian which comes from the Hamiltonian (8). The steps of this procedure are described in Caranicolas (1990) (see also Lichtenberg and Lieberman 1983). We give here the averaged Hamiltonian

$$\langle H \rangle = -\epsilon[25J + 625(\Lambda - J)\frac{(J+3\Lambda)}{2}] + 625\epsilon J(\Lambda - J)\cos 2\phi \tag{9}$$

and the map which is

$$\begin{aligned} J_{n+1} &= J_n + 1250\epsilon J_{n+1}(\Lambda - J_{n+1})\sin 2\phi_n \\ \phi_{n+1} &= \phi_n + \epsilon[625(\Lambda + J_{n+1}) - 25] + 625\epsilon(\Lambda - 2J_{n+1})\cos 2\phi_n \quad , \end{aligned} \tag{10}$$

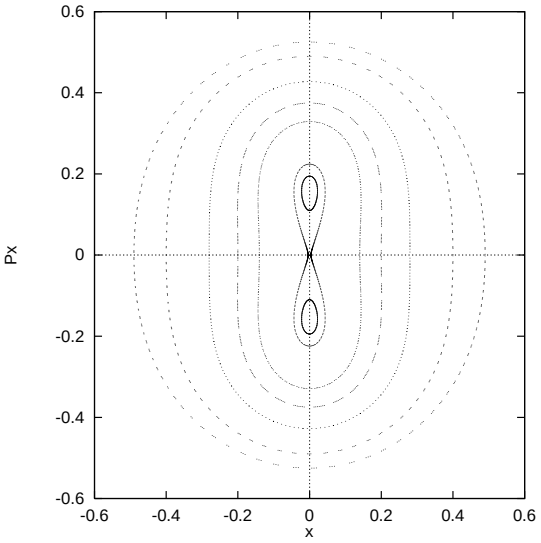

Fig. 1. Poincare surface of section generated by numerical integration when $\Omega = 0$. The values of h and ϵ are 0.125 and 0.0002 respectively.

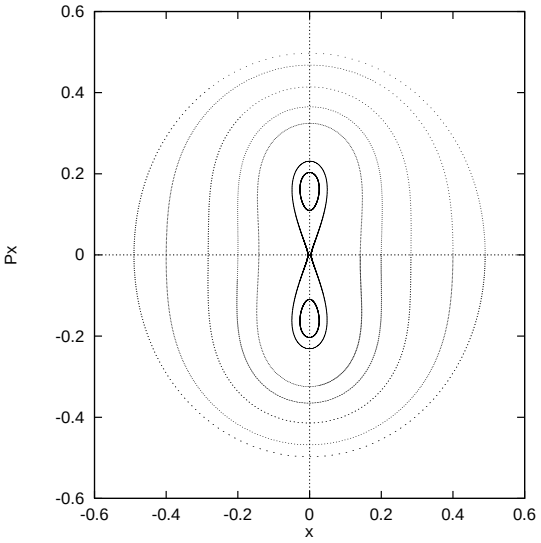

Fig. 2. Same as Fig. 1 generated by the map.

where $\Lambda = h$ and we return to x, p_x variables through $x = (2J)^{1/2}cos\phi$, $p_x = -(2J)^{1/2}sin\phi$. The fixed points of (10) are

$$\begin{aligned} &(i) \quad J = 0 \quad for \quad any \quad \phi \\ &(ii) \quad J = 1/75 \quad , \quad \phi = \pm\pi/2 \quad . \end{aligned} \tag{11}$$

Fig. 1 shows the (x, p_x) Poincare surface of section computed numerically while Fig. 2 shows the same surface of section generated by the map. The values of ϵ, Λ are 0.0002 and 0.125 respectively. As one can see the agreement between the two patterns is very good. Looking the surface of section of Fig. 2 we can see two families of orbits. (a) orbits with invariant curves surrounding the fixed point (i), that is the center and (b) orbits producing the small islands around the fixed points (ii). Orbits of type (b) stay close to the inclined straight-line periodic orbits passing through the origin. Orbits of type (a) are box

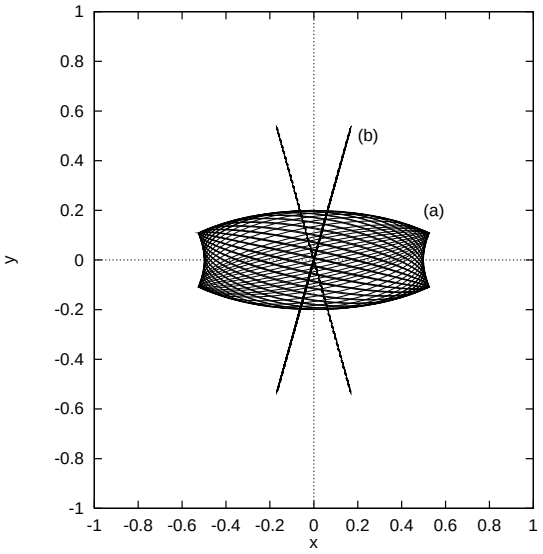

Fig. 3. Orbits of types (a) and (b) described in the text. The values of the parameters are as in Fig. 1.

orbits. The above two types of orbits are shown in Fig. 3. Note that the ellipses (1) which exist for small values of ϵ, become gradually box orbits for larger ϵ. It is evident that in both cases these orbits support the bar.

b) Rotating case

Now we proceed to study the properties of orbits in the rotating case. We consider the case where the bar rotates clockwise with angular velocity $\Omega > 0$. The Eqs. of motion are

$$\begin{aligned} \ddot{x} &= -2\Omega\dot{y} - \partial V_R/\partial x \\ \ddot{y} &= 2\Omega\dot{x} - \partial V_R/\partial y \end{aligned} \tag{12}$$

where the dot indicates derivative with respect to the time, $V_R = V - \Omega^2(x^2+y^2)/2$ while V is given by Eq. (5). For the convenience of our analysis we write V_R in the form

$$\begin{aligned} V_R &= \frac{1}{2}(Ax^2 + By^2) + \\ &\quad \alpha_1(\frac{1}{2}x^2y^2 + \frac{1}{4}y^4 - \frac{\epsilon}{\alpha_1}) - \frac{1}{50} \end{aligned} \tag{13}$$

where $A = 1-\Omega^2+50\epsilon$, $B = 1-\Omega^2+100\epsilon$ and $\alpha_1 = -2500\epsilon$. The corresponding Hamiltonian is

$$H_J = \frac{1}{2}(p_x^2 + p_y^2) + V_R = h_J \quad , \tag{14}$$

which is known as the Jacobi's integral and h_J is its numerical value.

If we consider only the quadratic terms, then the system of differential Eqs. (12) can be solved analytically(see Freeman 1966, De Zeeuw and Merritt 1983). The solution is

$$\begin{aligned} x &= C_1\cos(\omega_1 t + \psi_1) + \mu C_2 \sin(\omega_2 t + \psi_2) \\ y &= \nu C_1 \sin(\omega_1 t + \psi_1) + C_2\cos(\omega_2 t + \psi_2) \quad , \end{aligned} \tag{15}$$

where the constants C_1, C_2, ψ_1, ψ_2 are determined by the initial conditions. The frequencies $\omega_1 < \omega_2$ satisfy the quartic Eq.

$$\omega^4 - (A + B + 4\Omega^2)\omega^2 + AB = 0 \tag{16}$$

and

$$\mu = \frac{2\omega_2\Omega}{\omega_2^2 - A} \ , \ \nu = \frac{2\omega_1\Omega}{B - \omega_1^2} \quad , \quad |\mu| \le 1 \ , \ |\nu| \le 1 \tag{17}$$

In order to obtain the averaged Hamiltonian we use normal variables (q_1, q_2, p_1, p_2) defined by

$$\begin{aligned} q_1 &= (s\nu)^{1/2}[p_y + (\omega_2/\mu)x] \quad , \\ q_2 &= (s\mu)^{1/2}[p_x + (\omega_1/\nu)y] \quad , \\ p_1 &= (s/\nu)^{1/2}[p_x - \omega_2\mu y] \quad , \\ p_2 &= (s/\mu)^{1/2}[p_y - \omega_1\nu x] \quad , \end{aligned} \tag{18}$$

where

$$s = \frac{2\Omega}{\omega_2^2 - \omega_1^2} \quad . \tag{19}$$

In these variables the Hamiltonian (14) becomes

$$\begin{aligned} H_J &= \frac{1}{2}\omega_1(p_1^2 + q_1^2) + \frac{1}{2}\omega_2(p_2^2 + q_2^2) + \\ &\quad H_{1J}[q_1, q_2, p_1, p_2] \end{aligned} \tag{20}$$

Then we transform (20) to action-angle variables

$$\begin{aligned} q_i &= (2I_i)^{1/2}\cos\theta_i \\ p_i &= -(2I_i)^{1/2}\sin\theta_i \ , \ i = 1, 2 \end{aligned} \tag{21}$$

obtaining

$$\begin{aligned} H_J &= \omega_1 I_1 + \omega_2 I_2 + H_{1J}[I_1, I_2, \theta_1, \theta_2] = \\ &\quad H_{0J} + H_{1J}[I_1, I_2, \theta_1, \theta_2] \quad . \end{aligned} \tag{22}$$

The averaged Hamiltonian, describing the motion in the $J-\phi$ plane ($\theta_2 = \pi/2, \ \phi = \theta_1 - \pi/2$) (see also Caranicolas 1990), which is obtained from (22) writes

$$\begin{aligned} \langle H_J \rangle &= \frac{1}{2}k_1 J^2 + k_2 JR + \frac{1}{2}k_3 R^2 - k_4 S_1\cos\phi - \\ &\quad k_5 JR\cos 2\phi - k_6 S_2\cos\phi \quad , \end{aligned} \tag{23}$$

where

$$\begin{aligned} R &= (\Lambda_J - \omega_1 J)/\omega_2 \\ S_1 &= (J^3 R)^{1/2} \\ S_2 &= (JR^3)^{1/2} \end{aligned} \tag{24}$$

and

$$\begin{aligned} k_1 &= \frac{1}{4}\alpha_1(\frac{s}{\nu})^2[2\nu^2 + 3\nu^4] \quad , \\ k_2 &= \frac{1}{2}\alpha_1(\frac{s}{\mu})(\frac{s}{\nu})[1 + \mu^2\nu^2 + 3\nu^2] \quad , \\ k_3 &= \frac{1}{4}\alpha_1(\frac{s}{\mu})^2[2\mu^2 + 3] \quad , \\ k_4 &= \frac{1}{2}\alpha_1(\frac{s}{\mu})^{1/2}(\frac{s}{\nu})^{3/2}[\nu(1-\mu\nu) + 3\nu^3] \quad , \\ k_5 &= \frac{1}{4}\alpha_1(\frac{s}{\mu})(\frac{s}{\nu})[1 + 4\mu\nu + \mu^2\nu^2 - 3\nu^2] \quad , \\ k_6 &= \frac{1}{2}\alpha_1(\frac{s}{\mu})^{3/2}(\frac{s}{\nu})^{1/2}[3\nu - \mu(1-\mu\nu)] \quad . \end{aligned} \tag{25}$$

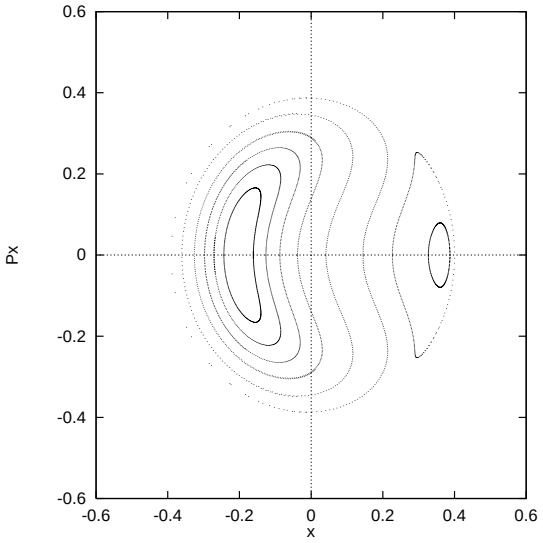

Fig. 4. Poincare $x - p_x$ surface of section generated by the map when $\Omega = 0.01$, $h_j = 0.125$, $\epsilon = 0.0002$.

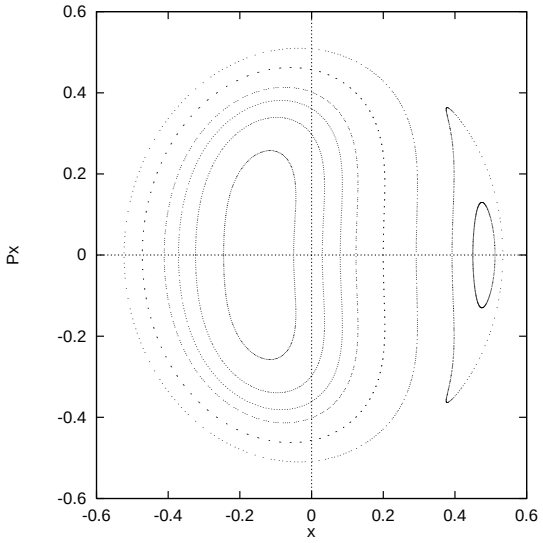

Fig. 5. Poincare $x - p_x$ surface of section generated by numerical integration when $\Omega = 0.01$, $h_j = 0.125$, $\epsilon = 0.0002$.

Note that in Eq. (23) we have set $H_{0J} = \omega_1 I_1 + \omega_2 I_2 = \omega_1 J_1 + \omega_2 J_2 = \Lambda_J = h_J$ and the constant terms have been omitted.

The positions of periodic orbits are given by

$$\begin{aligned} k_1 J \; + \; & \frac{1}{\omega_2} k_2(\Lambda_J - 2\omega_1 J) - k_3 \frac{\omega_1}{\omega_2} R \pm \\ & \frac{k_4 J^2}{2\omega_2 S_1}(4\omega_1 J - 3\Lambda_J) - \frac{k_5}{\omega_2}(\Lambda_J - 2\omega_1 J) \mp \\ & \frac{k_6}{2\omega_2 S_2}(\Lambda_J - 4\omega_1 J) R^2 = 0 \quad , \\ \phi \; = \; & 0 \; , \; \pi \quad , \end{aligned} \tag{26}$$

where the first value of ϕ and the upper sign correspond to retrograde orbits while the second value of ϕ and the lower sign correspond to direct orbits. The map describing the motion in $J - \phi$ plane is

$$\begin{aligned} J_{n+1} \; = \; & J_n - k_4 S_1 \sin\phi_n - 2k_5 J_{n+1} R \sin 2\phi_n \\ & - k_6 S_2 \sin\phi_n \\ \phi_{n+1} \; = \; & \phi_n + k_1 J_{n+1} + \frac{1}{\omega_2} k_2(\Lambda_J - 2\omega_1 J_{n+1}) - \\ & k_3 \frac{\omega_1}{\omega_2} R + g(J_{n+1}, \phi_n) \quad , \end{aligned} \tag{27}$$

where

$$\begin{aligned} g(J_{n+1}, \phi_n) \; = \; & \frac{k_4 J_{n+1}^2}{2\omega_2 S_1}(4\omega_1 J_{n+1} - 3\Lambda_J)\cos\phi_n - \\ & \frac{k_5}{\omega_2}(\Lambda_J - 2\omega_1 J_{n+1})\cos 2\phi_n - \\ & \frac{k_6}{2\omega_2 S_2}(\Lambda_J - 4\omega_1 J_{n+1}) R^2 \cos\phi_n \quad . \end{aligned} \tag{28}$$

Fig. 4 shows the surface of section generated by the map in the original variables x, p_x while the $x - p_x$ surface of section shown in Fig. 5 comes from numerical integration. The values of Ω, Λ_J, ϵ are 0.01, 0.125 and 0.0002 respectively. We return to the original variables through $q_1 = (2J)^{1/2}\cos\phi$, $p_1 = -(2J)^{1/2}\sin\phi$ and

$$\begin{aligned} x \; = \; & \frac{\mu(q_1\sqrt{s/\mu} - p_2\sqrt{s\nu})}{\sqrt{s/\mu}\sqrt{s\nu(\mu\nu\omega_1 + \omega_2)}} \quad , \\ p_x \; = \; & \frac{p_1\omega_1}{\sqrt{s/\nu}(\omega_1 + \mu\nu\omega_2)} \quad , \end{aligned} \tag{29}$$

where $p_2 = -c_1(2I_2)^{1/2} = -c_1(2R)^{1/2}$ and $c_1 = |\alpha_1/2|$. The choice of c_1 is justified by the fact that the quantities q_1, p_1, entering Eqs. (29), come from the averaged Hamiltonian (23) which is proportional to $\alpha_1/2$ while p_2 comes from H_0. Multiplying by c_1 makes p_2 of the same order of magnitude as q_1 and p_1. As one can see the map describes satisfactorily the general characteristics of orbits for small Ω. This is interesting because it shows that we do not lose much information- while averaging and also because the surface of section $\theta_2 = \pi/2$ does not coincide with the surface of section $y = 0$, as it does in the non rotating case. The patterns shown in Figs. 6 and 7 are generated by the map and numerical integration. The values of Λ_J, ϵ are as in Figs. 4 and 5 but $\Omega = 0.15$. We observe that again the map describes satisfactorily the characteristics of orbits.

We can see two families of orbits. The first family is the one that forms invariant curves surrounding the direct periodic point while the invariant curves of the second family surround the retrograde periodic point. The corresponding orbits, in both cases, are tube orbits. Note that box orbits are not present. Fig. 8 shows two orbits starting near the direct (d) and retrograde (r) periodic orbits. The values of the parameters are as in Fig. 5.

4. Chaotic motion

In this Sect. we shall study the onset of chaotic motion in our galactic potential in both rotating and non rotating case. This is of interest, because it gives information for the kind of motion

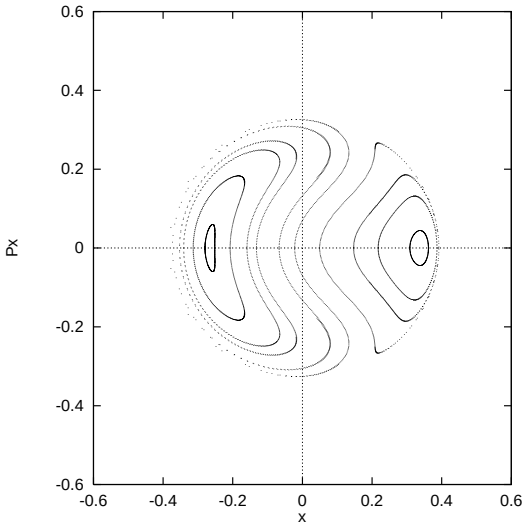

Fig. 6. Poincare $x - p_x$ surface of section generated by the map when $\Omega = 0.15$, $h_j = 0.125$, $\epsilon = 0.0002$.

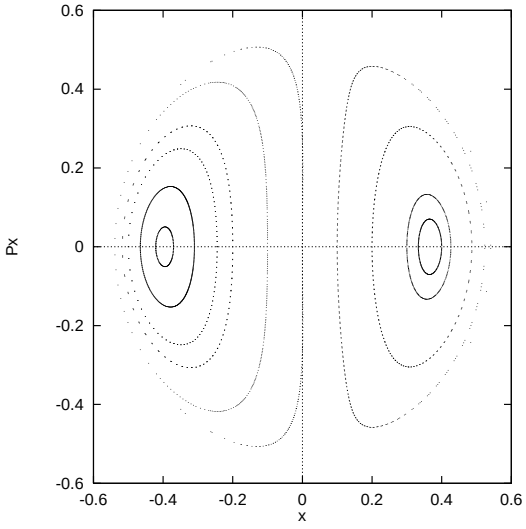

Fig. 7. Poincare $x - p_x$ surface of section generated by numerical integration when $\Omega = 0.15$, $h_j = 0.125$, $\epsilon = 0.0002$.

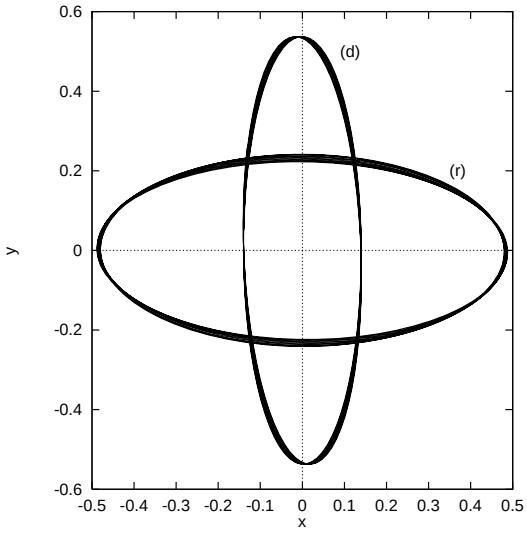

Fig. 8. Orbits starting near the direct (d) and the retrograde (r) periodic orbits. The values of the parameters are as in Fig. 5

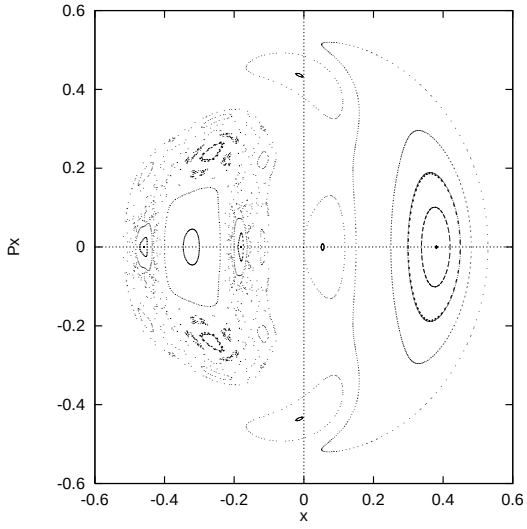

Fig. 9. Poincare $x - p_x$ surface of section when $\Omega = 0.2$, $\epsilon = \epsilon_{esc.}$, $h_J = 0.125$. A significant part of the surface of section is covered by chaotic orbits.

in the central parts of bar galaxies and shows how this is affected by the angular velocity Ω. Furthermore the results of this study will be compared with those observed in strong bars. Generally speaking, for a given value of energy one must go to the escape perturbation parameter ϵ_{esc} in order to observe chaos. This is given by

$$h_J + \frac{1}{50} + \frac{A}{5000\epsilon}(\Omega^2 - 1) + \epsilon(1 - \frac{A}{100\epsilon})^2 = 0 \qquad (30)$$

and can be found following the method described in Caranicolas and Varvoglis (1984). In the following we present results for $h_J = 0.125$ and several values of Ω at ϵ_{esc}. When $\Omega = 0$ only signs of chaos are observed near the hyperbolic periodic point at the center. When $\Omega = 0.01$ no chaotic motion is observed. At $\Omega = 0.1$ signs of chaos appear at the area of direct orbits which increases at $\Omega = 0.2$ (see Fig. 9). The chaotic area decreases at $\Omega = 0.3$ and at $\Omega = 0.4$ the motion is again regular. We see that this is an interesting behavior. On the other hand this behavior is different from that observed in strong bars (see Caranicolas and Karanis 1998). The main points are the following:

(i) The degree of chaos in all cases is higher in strong bars than in weak bars. In other words, in strong bars one speaks about a chaotic layer of significant width while in weak bars, the area on the surface of section covered by chaotic orbits, is much smaller in general.

(ii) In the strong bar examined in Caranicolas and Karanis (1998) the degree of chaos decreases as Ω increases and finally at $\Omega = 0.225$ all orbits are regular. Here, at small Ω, there is no chaotic motion, then chaos increases as Ω increases, reaches a maximum at about $\Omega = 0.2$ and finally all orbits are regular at about $\Omega = 0.4$.

5. Discussion

The aim of this research was to make a paper with a compound character. We have tried to avoid the details and present the main results, which is the substance of this investigation. First we started with a family of ellipses. Similar ellipses were observed in a self consistent model of interacting galaxies. N-body simulations have shown that the above orbits form a bar structure. On the basis of the Theory of the Inverse Problem (see for further details a review by Bozis 1995) we have constructed a simple potential, which represents a weak bar structure. Such potentials made up of harmonic oscillators have been extensively used in order to model galaxies near an equilibrium point (see Caranicolas 1993, 1994 and references therein).

In order to see the properties of orbits in this potential we constructed a map. Maps are very useful for the study of the properties of motion in dynamical systems, because they are not only elegant but also faster, in general, than numerical integration. Useful information on maps can be found in Lichtenberg and Lieberman (1983).

We have studied the $x - p_x$ surface of section in the non rotating case. The agreement with numerical integration is very good even for large values of ϵ $(\epsilon \leq \epsilon_{esc})$. In this case the general characteristic of motion is, that nearly all orbits are box orbits. On the other hand, in the rotating case, things appear more complicated. This complexity comes from the fact that the surfaces of section $y = 0$ and $\theta_2 = \pi/2$ do not coincide, as they do when $\Omega = 0$. Nevertheless it was observed, that the general characteristics of motion are satisfactorily described, if we consider the $\theta_2 = \pi/2$, surface of section and return to the original variables $x,\ p_x$ using (29). Note that the results are satisfactory even for large values of Ω, such as $\Omega = 0.15$.

Both in strong and weak bars, chaos was observed when the value of the perturbation parameter is very close to the ϵ_{esc}. In the case of weak bars the degree of chaos is much more smaller than that observed in strong bars. Both strong and weak bars do not show chaos when $\Omega > \Omega_{cr}$. This Ω_{cr} seems to be larger in weak than in strong bars.

It is evident that the conclusions given in this research refer to strong and weak bars represented by perturbed harmonic oscillators. It is well known that the motion described by harmonic oscillators is local. In other words, potentials (5) and (13) do not represent a barred galaxy as a whole but a non-rotating or a rotating isolated bar. Therefore the above equations can be considered as an approximate description for the real potential of the central parts of a barred galaxy. Thus, the outcomes of this research refer to local motion. The global motion in barred galaxies has been extensively investigated by many authors and the reader can find interesting information in their works (see e.g. Contopoulos and Papayannopoulos 1980, Pfenniger and Friedli 1991, Papaphilipou and Laskar 1998 and the review paper by Contopoulos and Grosbol 1989).

Acknowledgements. This work was supported by the greek research program PENED N^o 1744. Our thanks go to an anonymous referee for his useful suggestions.

References

Binney, J., Tremaine, Sc., 1987, Galactic Dynamics, Princeton University Press
Bozis,G., 1995, Inverse Problems 11,687
Bozis,G., Borghero,F., 1997, Potenziali compatibili, con famiglie di orbite data in forma parametrica in XII Congresso Nationale Associaziona Italiana Di Meccanica Teoreca ed Applicata, Siena 29 Sept-3 Ott. ed Prof: Pierro Villagio
Caranicolas, N.D., 1990, Cel. Mech. 47,87
Caranicolas, N.D., 1993, A&A 267,368
Caranicolas, N.D., 1994, A&A 287,752
Caranicolas, N.D., 1998, A&A 332,88
Caranicolas, N., Varvoglis, Ch., 1984, A&A 141,383
Caranicolas, N.D., Karanis, G.I., 1998, A&SS (in press)
Caranicolas,N.D, Innanen, K.A., 1992, A.J. 103,1308
Combes, F., Dupraz, C., Gerin, M., 1990, in Dynamics and Interactions of Galaxies, p. 205, Ed. R. Wielen, Springer-Verlag Berlin,Heidelberg
Contopoulos, G., Grosbol, P., 1989, A&A Review 1, 261
Contopoulos, G., Papayannopoulos, T., 1980, A&A 92, 33
Deprit, A., 1991, Cel. Mech. 51, 203
De Zeeuw, T., Merritt, R., 1983, Ap.J 267,571
Freeman, K.C., 1966, M.N.R.A.S 133,47
Lichtenberg, A.J., Lieberman, M.A., 1983, Regular and stochastic motion,Springer,Berlin Heidelberg, New York
Miller, R., Smith, B.F., 1979, A. J. 227,785
Miwa, T., Noguchi, M., 1998, Ap.J. 499, 149
Papaphilipou, Y., Laskar, J., 1998, A&A 329, 451
Pfenniger, D., Friedli, D., 1991, A&A 252,75